Received: 14 September 2023 | Revised: 27 October 2023 | Accepted: 3 November 2023

DOI: 10.1002/jms.4986

RESEARCH ARTICLE

Journal of MASS SPECTROMETRY WILEY

Modelling some rod set imperfections of a quadrupole mass filter

Pavel V. Bugrov[1,2] | Aleksey A. Sysoev[1] | Nikolai V. Konenkov[1,2]

[1]Laboratory of Applied Ion Physics and Mass Spectrometry, National Research Nuclear University MEPhI (Moscow Engineering Physics Institute), Moscow, Russia

[2]Laboratory of Quadrupole Mass Spectrometry, Ryazan State University named after S.A. Esenin, Ryazan, Russia

Correspondence
Nikolai V. Konenkov, Laboratory of Applied Ion Physics and Mass Spectrometry, National Research Nuclear University MEPhI (Moscow Engineering Physics Institute), Kashirskoe Sh. 31, Moscow, Russia.
Email: n.konenkov@365.rsu.edu.ru

Funding information
Ministry of Science and Higher Education of the Russian Federation, Grant/Award Number: 075-03-2023-097

Abstract

The problem of modeling the mass peak shape of a quadrupole mass filter (QMF) with round rods is considered. A number of factors leading to the degradation of the mass peak shape are studied, namely, displacement of the electrodes with respect to their original position, changes in the diameter of the electrodes, and asymmetry of the supply potentials. Decomposition of the rod set field on multipole fields allows to obtain an analytical representation of the ion motion equations. Simulations have shown that a parallel shift of one or two electrodes leads to a shift of the peak along the mass number axis and dips at the peak apex. Unbalance of supply voltages does not significantly distort the peak shape, but it shifts the peak along the mass axis and creates a jump of the quadrupole offset potential proportional to the relative unbalance $\Delta V/V$ of X and Y rods potentials.

KEYWORDS
mass peak shape, mass shift, quadrupole mass filter, round rods, spatial harmonics

1 | INTRODUCTION

The shape of the mass peak reflects the analytical capabilities of the quadrupole mass filter. It is influenced by many factors such as the imperfection of electrodes and their assemblies, input fringing fields, coupling of the source of ions and the analyzer, the ion separation time, energyspread as well as low-frequency and high-frequency electrical field inductions on the QMF electrode circuit.[1] In addition, the focusing and imaging properties of the quadrupole field can influence the peak shape.[2–4]

Many companies use round electrodes instead of electrodes with hyperbolic profile. Technology of manufacturing and assembly of cylindrical electrodes with micron error is much cheaper than for rods with hyperbolic section. The use of imperfect manufactured QMFs with circular rods leads to appearance of regular dips in the mass peaks.[5–13] This is explained by the fact that the circular cross section electrodes produce nonlinear resonances.[14–16]

The parameter r/r_0 determines the construction of the QMF where r is the rod radius and r_0 is the radius of the inscribed circle between the electrode tips. According to last data[7,17] optimal range is $r/r_0 = 1.125–1.130$. Many numerical methods of computing accurate 3D fields for prediction of the effects of imperfect QMF construction were developed by Gibson and Taylor.[7–12] Ions with a uniform distribution across the field aperture and randomly placed with respect to the rf phase were used.[8–12] The most common defects are those of wrongly positioned rods and rods that do not have identical diameters. The boundary element method (BEM) have been used to study the effects of the source gap on transmission efficiency.[18] The authors solved the problem of numerical simulation of the input boundary element fields in order to optimize the QMF transmission.

Solving the Laplace equation numerically for calculating the electric field and trajectories of ions is a computationally intensive problem.[3,5–12] An alternative approach is to expand the field of round rods into a convergent series of harmonic polynomials (multipole fields). Methods for calculating the weighting factors are presented.[19,20] Setting the geometry of four parallel cylindrical electrodes, one can easily calculate the weighting factors A_K (amplitudes of spatial harmonics) for higher-order terms. The problem of systematic calculation of trajectories in analytical fields is simplified by using Runge–Kutta of order 8. The limitation of this method as compared to solving the Laplace equation numerically is the requirement for rods to be parallel.

The study of the mass peak shape on the base of the spatial field harmonics is the goal of the present work. Changes in the electrode radius, their displacement relative to the initial positions leads to a change in the composition of spatial harmonics. The composition and amplitude of spatial harmonics can be used to make conclusions about nonlinear resonances, which lead to the appearance of regular dips in the mass peaks. Fourteen field terms of order K = 2, 3, ..., 14 generated by circular electrodes were taken into account when modeling the peak shape.

2 | MASS PEAK CALCULATION METHOD

The electric potential $\Phi(x,y,t)$ generated by the four parallel electrodes of the QMF when a sinusoidal voltage $V_m \cos\Omega t$ and a constant voltage U are applied to the electrodes is[20]

$$\Phi(x,y,t) = Re\left[\sum_{K=2}^{14} A_K \left(\frac{x+iy}{r_0}\right)^K\right](U+V_m\cos\Omega t), \quad (1)$$

where V_m is the amplitude of RF voltage, $z=x+iy$ is the complex coordinate, r_0 is the radius of the inscribed circle between the electrode tips, Ω is the angular frequency, $i=\sqrt{-1}$, A_K is the weighting factor for K pole multipole field. Explicit formula for potential (1) allows to write equations of ion motion in analytical form. The ion trajectory method was used to calculate the peak shape. To calculate the trajectories of ions Wolfram Mathematica-10[21] is used. The ion motion equations in dimensionless variables has the form:

$$x''(\xi) + \left[\frac{a}{2} + q\cos(2(\xi-\xi_0))\right]\frac{\partial}{\partial x} Re\left[\sum_{K=2}^{14} A_k (x+iy)^K\right] = 0, \quad (2)$$

$$y''(\xi) + \left[\frac{a}{2} + q\cos(2(\xi-\xi_0))\right]\frac{\partial}{\partial y} Re\left[\sum_{K=2}^{14} A_k (x+iy)^K\right] = 0. \quad (3)$$

Here, x and y are the transverse coordinates normalized to r_0, $\xi = \Omega t/2$ is the dimensionless time, ξ_0 is the initial phase of the ion arrival in the rf field and a and q are the dimensionless parameters:

$$a = \frac{8eU}{(m/z)r_0^2\Omega^2},\ q = \frac{4eV}{(m/z)r_0^2\Omega^2}, \quad (4)$$

where e is the proton charge, m/z is the ion mass m divided on degree z of ionization, U is the DC potential, V_m is the RF amplitude, r_0 is the "field radius," Ω is the angular frequency. The dimensionless standard deviation of velocities along the transverse X and Y coordinates is determined by the formula[22]:

$$\sigma_v = \sqrt{2R_g\frac{T_i}{\mu}}\frac{2}{r_0\Omega}, \quad (5)$$

where $R_g = 8.314\,m^2\ kg\ c^{-2}\ K^{-1}\ Mol^{-1}$ is the universal gas constant, T_i is the ion temperature, μ is the molar mass. We took the following values in calculations: $T_i = 300\,K$, $\mu = 609\,kg/kmol$, $r_0 = 0.005\ m$, $f = 2\pi/\Omega = 1$ MHz. The dimensionless standard deviation σ_x for transverse coordinates in units of r_0 was set in the range of 0.01–0.3. Note that the standard deviation σ_x characterizes the radial distribution of the ion ensemble, which is subject to nonlinear resonance.[20] The scan parameter $\lambda = a/2q = U/V$ is calculated using expression $\lambda = 0.16784 - 0.1261/R$ from.[1, p.23] Basic data input to the program were the initial conditions, the separation time n (number RF cycles which ion spend in RF field), the number N of trajectories per point for graph in Figure 1. It was used $N = 10\,000$ and $P = 30$ points for graph.

3 | MASS PEAK SHAPE

Here, we study influence of the r/r_0 parameter on the mass peak shape. Figure 1 shows the result of numerical simulation of the peak shape for the indicated parameters $r/r_0 = 1.125$–1.145 and for two models of the input ion beam. The input beam is a Gaussian beam which is characterized by the coordinate standard deviation $\sigma_x = \sigma_y = 0.01r_0$ and transverse velocity standard deviation $\sigma_V = \sigma_{Vx} = \sigma_{Vy} = 0.0126\pi r_0 f$ for ions with $m/z = 609\ Th$ and temperature $T_i = 300\,K$. The *ion transit time* through the *mass filter* $n = 150$ RF cycles. The shape of the peaks is substantially asymmetric and roughly triangular. The intensity of the peaks changes slightly with resolution $R = q/\Delta q = 609$ ($\lambda = 0.1676$) excluding the case $r/r_0 = 1.145$. A weak dip is observed at the tops of the peaks.

Figure 1B shows that under similar conditions the shape of the peaks when the input beam is parallel and the distribution of the initial coordinates has the standard deviation $\sigma_x = 0.01$. This corresponds to the case of a degenerate QMF acceptance, when its area is zero. The use of such an input beam model gives an increase of approximately 18% in the transmission. The peak shape also contains weak dips. The hexapole term of the field $A_6 \cong 0$ for $r/r_0 = 1.145$. As a result, the field harmonics with amplitudes $A_2 = 1.002754$, $A_{10} = -0.002429$ and $A_{14} = -0.000283$ gives a broadened peak with lower transmission. Removing the positive hexapole component of the field does not improve the peak shape, resolving power or transmission. However, the combination of the 6th, 10th and 14th field harmonics improves the QMF performance due to that the amplitudes A_6 and A_{10} have opposite signs.

Figure 2A shows the peak shape for combinations of quadrupole harmonic $A_2 = 1.00141968$ with hexapole $A_6 = 0.00133436$, with dodecapole $A_{10} = -0.002430$ and with quattuordecimpole $A_{14} = -0.00029798$ and for rod set with $r/r_0 = 1.125$ at large ion filling of mass filter characterized by the standard deviation $\sigma_x = 0.3$. Because the QMF acceptance (the region on the phase plane of admissible transverse coordinates and velocities) decreases rapidly with increase of resolving power,[1] the QMF transmission decreases from 60% to 2.5%. Each pair of components (term 2 + term K) yields vastly different mass peaks in shape, transmission, and resolution. The best peak

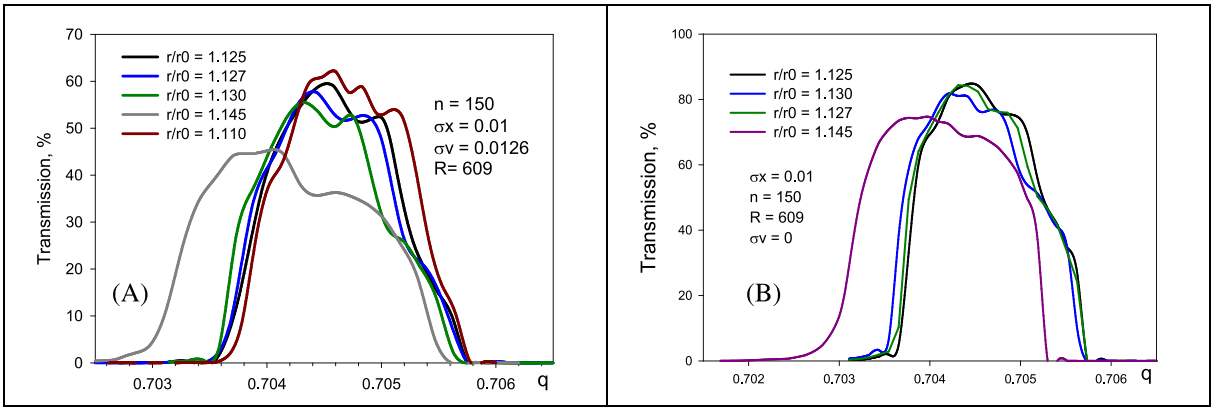

FIGURE 1 Calculated peak shape for four values of the design parameter $r/r_0 = 1.110$, 1.125, 1.127, 1.130 and 1.145. (A) Gaussian ion beam: M = 609 Th, $T_i = 300\,K$, $\sigma_x = 0.01$. (B) Input parallel ion beam with Gaussian radial distribution: $\sigma_x = 0.01$. The resident time through quadrupole is 150 RF cycles.

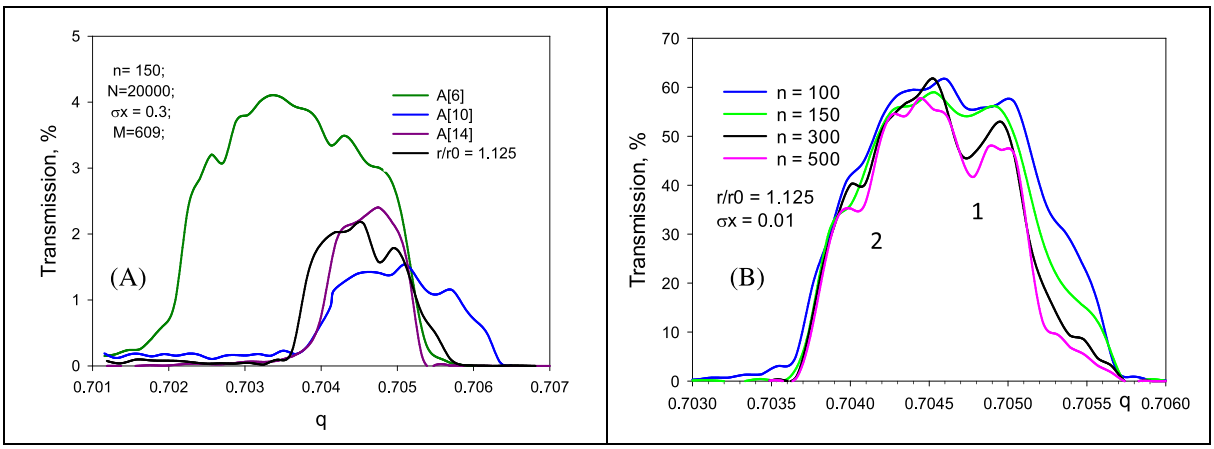

FIGURE 2 (A) Effect of individual multipole components on the mass peak shape. (B) Increase in the dips' depth in the transmission contour at the indicated values of the ion separation time *n*.

shape is given by a combination of strong quadrupole and weak dodecapole components.

The effect of ion separation time *n* on the shape of the peak is illustrated in Figure 2B. What is significant here is that the intensity of the dips' depth on the graph increases with time *n*. This corresponds to the results.[6–10] A second dip appears on the left side as time *n* increases. This indicates that the cause of the dips is nonlinear resonances on the hexapole and dodecapole spatial harmonics.[16,17]

At relatively low resolution, regular dips are not observed even at r/r_0=1.148.[7] Figure 3A,B shows the mass peaks for two values of the design parameter r/r_0=1.125 and r/r_0=1.127 for low resolution R = 45 and small sorting time $n = 65$. It can be seen that there are no significant manifestations of nonlinear resonances. The absence of regular dips at low-mass ions is possibly due to the fact that the resonance band on the *a*,*q* parameter plane is much narrower than the Δq QMF bandwidth for small ion separation time *n*.

4 | IDENTIFICATION OF THE DIPS

The dips on the mass peak contour characterize the quality of rod set fabrication and assembly. Identification of dips (manifestation of nonlinear resonances) on the transmission contour can be useful in debugging the technology of quadrupole manufacturing. Our goal here is to identify regular dips 1 and 2 (Figure 2B), caused by nonlinear resonances.[14–16] According to the results of[15,16] the following resonance lines passing through the top of the QMF stability diagram can be distinguished. The resonance lines are most intense when they simultaneously belong to nonlinearities of order 6 and 10[15,16]:

$$\beta_x \pm \beta_y = 1;\ \beta_x \pm 2\beta_y = 1 \text{ and } \beta_x \pm 4\beta_y = 1; \quad (6)$$

From Figure 2B, we can determine the coordinates of dip 1 on the QMF transmission contour. By a direct measurement with a

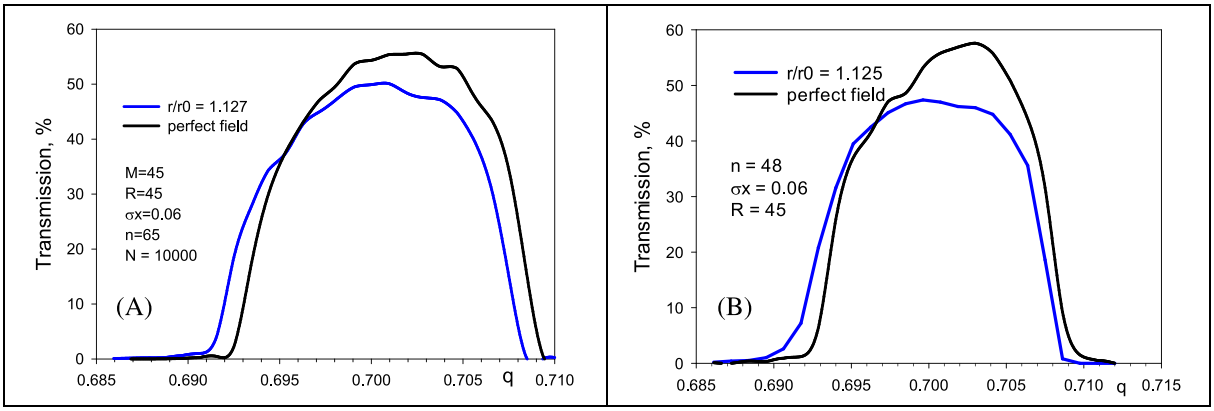

FIGURE 3 Transmission contour shape for two values of the design parameter r/r_0=1.127 (A) and $r/r_0 = 1.125$ (B) for ions with mass M = 45 Th.

marker, we find the coordinate $q = 0.704764$. Knowing the value of $\lambda = 0.1676\,(R = 609)$, we find the coordinate $a = 2\lambda q = 0.2362$. Using the values of parameters a,q, we determine that $\beta_x = 0.966292$ and $\beta_y = 0.002712$. None of the inequalities (6) is satisfied for the found β_x and β_y. This is due to the fact that the stability diagram of the Mathieu equation is modified by the presence of multipole fields.

To establish the resonances responsible for the dips, the ion escape beyond the confinement region $x^2 + y^2 < 1$ was calculated as a function of the parameter q in the absence of a constant potential $U\,(a = 0)$ (Figure 4). This dependence was calculated for $r/r_0 = 1.125$, $\sigma_x = 0.2$ and long sorting time $n = 3000$ RF cycles (Figure 4). Here, amplitudes $A_6 = A_{10} = 0.004$ are slightly increased compared to the initial $A_6 = 0.0013$ and $A_{10} = -0.0024$. Under typical conditions of Figure 2B, the resonant peaks are vanished in the noise. Intensity of resonance peaks has a cumulative character with respect to time.[20] We distinguish four resonance peaks with coordinates $q = 0.344$, 0.451, 0.369 and 730. These coordinates correspond to β values 1/5, 1/3, 1/2, 3/10 and 3/4. It is worth noting that when $a = 0$ frequency parameters $\beta_x = \beta_y = \beta$.

From here we get that the peak $\beta = 1/5$ determines the resonance curve $\beta_x + 4\beta_y = 1$, $\beta = 1/3$ is the curve $\beta_x + 2\beta_y = 1$, $\beta = 1/2$ is the curve $\beta_x + \beta_y = 1$. Resonances of order 10 $\beta = 3/10$ and $\beta = 3/4$ are small compared with the peaks 0.451 and 0.639. Thus, it can be argued that the central dip 1 (Figure 2B) is due simultaneously to resonances for harmonics of order 6 and 10 that gives resonance curve $\beta_x + \beta_y = 1$. The edge resonance (dip 2, Figure 2B) can be attributed to the resonance curve $\beta_x + 2\beta_y = 1$.

5 | AXIAL OFFSETS AND DEVIATIONS OF ELECTRODE DIAMETERS FROM THEIR NOMINAL VALUE

The effect of X or Y displacement of the rod at distances $\pm 0.005 r_0$ from the original position is shown in Figure 5. The "+" sign corresponds to the displacement of the electrode from the quadrupole center. In the case of $A_2 < 1$, the mass peak shifts to the right

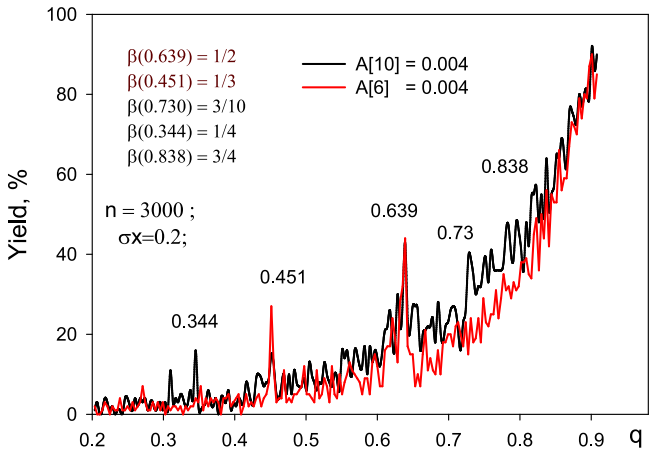

FIGURE 4 Resonance yield of ions as a function of parameter q at $a = 0$ for two multipoles with amplitudes of (A) $A_6 = 0.004$ and (B) $A_{10} = 0.004$. Separation time $n = 3000$ RF cycles.

along the q axis (toward large masses) relative to its original position. Displacement of the X and Y electrodes to the center gives $A_2 > 1$. This leads to a shift of the mass peak by approximately 1Th toward the low masses. The magnitude and sign of the shift is determined by the amplitude A_2. For the case when the field radius $r_0 = 0.5\,cm$ displacement is $0.005 r_0 = 25\,\mu m$. This only shifts the peak by $\pm Th$ at resolution of $R \approx 600$ without loss of mass peak quality.

The effect of simultaneous displacement of X or Y electrodes on the shape and displacement of the peak and are shown in Figure 6. Shifting the two X electrodes (Figure 6A) toward the center of the quadrupole shifts the peak to the left along with a slight increase in transmittance. Shifting the two X electrodes away from the center gives a shift of the peak to the right along the q-axis with a slight increase in resolution. A similar pattern occurs when the Y electrodes are shifted simultaneously (Figure 6B). Shifting the Y electrodes toward the center along q-axis gives a peak with increased resolution and a small loss of transmittance without an obvious dip at the apex of the peak.

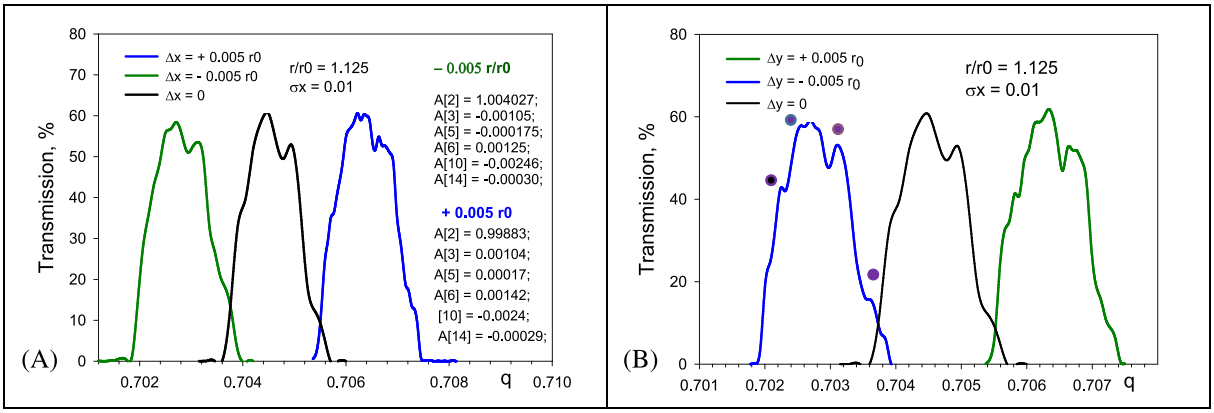

FIGURE 5 (A) Displacement of one X rod in positive and negative directions by distance $\Delta x = \pm 0.005 r_0$; (B) displacement of one Y rod by distance $\Delta y = \pm 0.005 r_0$ from the original position. $r/r_0 = 1.125$.

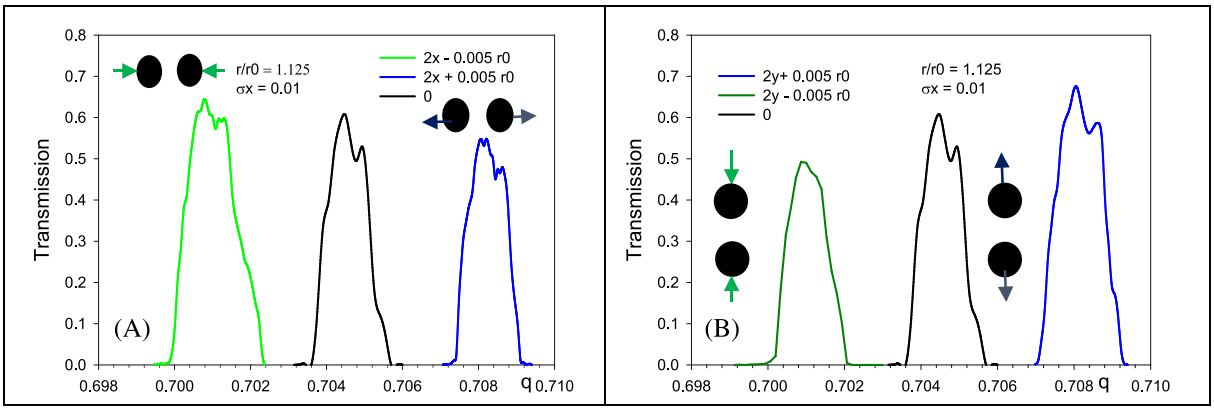

FIGURE 6 Symmetrical displacement of two X (A) and Y (B) rods simultaneously inside and outside the analyzer by $\Delta x = \Delta y = \pm 0.005 r_0$ from their nominal position, $r/r_0 = 1.125$. The arrows indicate the displacement of opposite rods.

Figure 7 shows the effect of the size of the radius of one X or Y electrode when each is changed by $\pm 0.005 r_0$ for the QMF design parameter $r/r_0 = 1.125$. As before, if $A_2 > 1$ then the shift of the peak is toward small q, if $A_2 < 1$, the shift of the peak is toward larger values of q. Increasing the X electrode radius results in increasing the peak intensity and its broadening, while decreasing it results in a slight decrease in the peak intensity and its shift to the right along the q-axis.

Increasing the radius of one X electrode (r_x=1.130) from the nominal ($r_0 = 1.125$) results in a shift of the peak to the left along the q-axis with an increase in transmission. Decreasing the radius of this electrode (r_x=1.120) gives decrease in transmission and a slight shift in peak. Decreasing the radius of Y electrode (r_y=1.120) hardly changes the peak position and increasing it (r_y=1.130) shifts the peak with decreasing transmission.

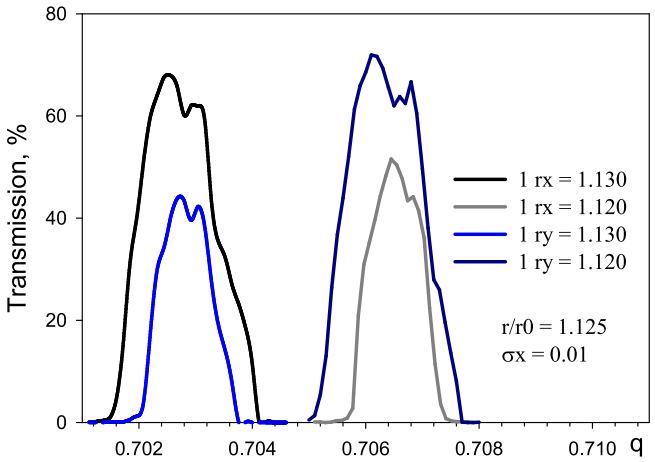

FIGURE 7 Effect of the X and Y radii of the rods $(1.125 \pm 0.005) r_0$ on the shape of the mass peak.

6 | UNBALANCE OF SUPPLY VOLTAGES

Feeding X and Y electrodes of QMF with potentials $V_x = V - \Delta V$ and $V_y = -V - \Delta V$ results in the mass peak not shifting along the mass scale, but the quadrupole Z axis potential will be $V_0 = (-\Delta V - \Delta V)/2 = -\Delta V$.[19] It means that ions will experience a potential jump of $-(\Delta V/V)(U + V_m \cos \Omega t)$ at the entrance to the

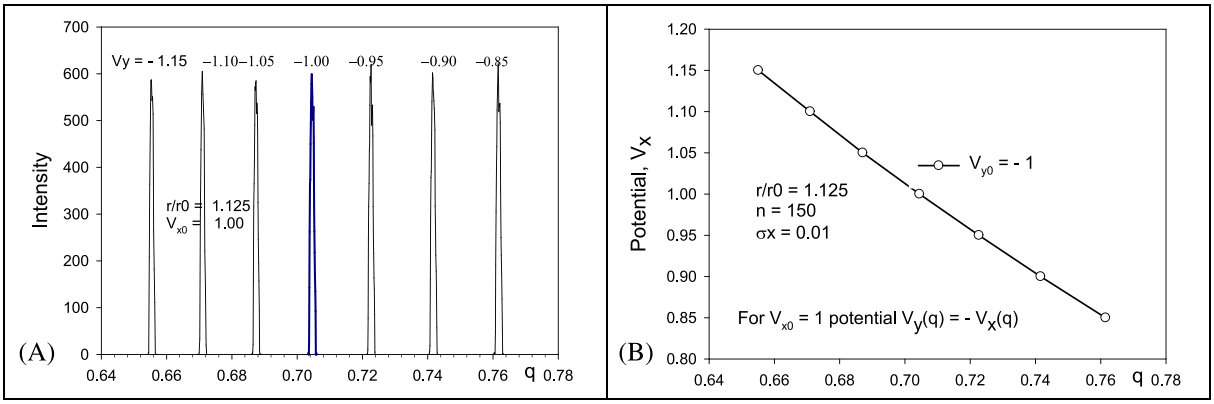

FIGURE 8 (A) Shift of the peak position along the *q axis* when changing the potential $V_y = -1.15, \ldots, -0.85$ at constant X potential $V_{x0} = 1$. (B) Position of the peak on the *q*-axis when the potential $V_x = 0.85, \ldots, 1.15$ changes and the Y potential $V_{y0} = -1$ is constant, normalized to $U + V\cos\Omega t$.

quadrupole boundary field, which can lead to ion scattering and loss of transmission. When fed with potentials $V_x = V + \Delta V$ and $V_y = -V + \Delta V$ the quadrupole will have the Z axis potential $V_0 = +\Delta V$, where ΔV is disbalance potential at the electrodes. A previously performed experiment[23] shows that at RF potential imbalance when DC potential $U_x = U_y$ the output signal of $C_4F_9^+$ ions ($m/z = 219$) drops sharply at $\Delta V \approx 20\,Volts$.

The position of the mass peak along the q axis is shown in Figure 8A for a series of Y potential values $V_y = -1.15, \ldots, -0.85$ at constant potential $V_{x0} = 1$. It can be seen that the asymmetry of the X and Y supply voltages results in a shift of the mass peak to the left along the mass scale for $V_y < 1$. The shape of the peak does not change significantly. Figure 8B shows graphically the effect of the V_x potential on the position of the mass peak along the q coordinate at $V_{y0} = -1$. For $V_{x0} = -1$, $V_y(q) = -V_x(q)$.

7 | DISCUSSION AND CONCLUSION

Modeling of the mass peak shape of QFM with cylindrical electrodes on the basis of electric field potential description with terms of order $K = 2, 6, 10, 14$ revealed a presence of a weak regular peak for the case of resolving power about $R = 600$. The presence of regular dips for the QMF design parameters $r/r_0 = 1.110, 1.125, 1.127, 1.130$ is explained by nonlinear resonances at the frequencies of spatial harmonics. The weak dip is caused by the main resonance line $\beta_x + \beta_y = 1$, which crosses the top of the stability diagram. At small values of resolving power $R = 45$, the dip on the mass peak is not detected. The width and intensity of the resonance line strongly depend on the time n and the radial ion density characterized by σ_x.[15,20] In our case, the nonlinear resonance is undetectable even for the case when $a = 0$. This means that the bandwidth Δq of the QMF is very narrow for $R = 600$ and comparable to the resonance bandwidth Δq_{res}. In the case of low resolution $R = 45$, the banwidth $\Delta q_{res} \ll \Delta q$, so no resonant band is observed. In a real experiment, many factors distort the mass peak shape. These include coupling of ion source and analyzer, ion energy, input fringing fields, focusing and imaging properties of the quadrupole field, and also difficult to control factors like barrel-shaped, non-parallel electrodes.

Moving one X or Y electrode on $\Delta = 25$ μm for electrode diameter of 5.000 mm does not distort the peak shape notably and only shifts the peak on the mass scale. This is in contradiction with the simulation results when $0.005r_0$ moves one Y electrode inward r_0.[11] The calculated mass peaks,[11] Figure 4A have large dips. In Figure 4B, we can also observe four weak dips. We attribute this difference to different methods for quadrupole field simulation. Simultaneous displacement of two X electrodes in opposite directions by $0.005r_0$ results in mass peak shift also in opposite directions along the q axis.

Decreasing the radius of one X or Y rod by $0.005r_0$ leads to a peak shifting to the right along the q axis. Increasing the radius further leads to a shift to the left along the q axis. The direction of the shift is determined by the value of the weighting factor A_2: for $A_2 < 1$, the shift is to the right along the q axis, for $A_2 > 1$, the shift is to the left. This peak shift on the mass scale is eliminated by calibration to a known mass spectrum. Asymmetrical potential imbalance at the opposite electrodes of the type $V_x = V - \Delta V$ and $V_y = -V - \Delta V$ does not lead to a mass peak shift, but the potential of the whole quadrupole changes by $-(\Delta V/V)(U + V_m\cos\Omega t)$, $-\Delta V$ share from the unity potential $V = 1$. With another imbalance $V_x = V + \Delta V$ and $V_y = -V + \Delta V$ the quadrupole will acquire positive potential $+(\Delta V/V)(U + V_m cos\Omega t)$. It results in a transmission loss of the mass filter.[23]

It's worth noting that the mode of ion separation in stability islands improves the peak shape and resolution and is a method to overcome a wide range of field imperfections in quadrupole mass filters.[24] In another paper[25] a quadrupole mass spectrometer (QMS) designed for space exploration is described. It has a separation mode in the upper stability island created by resonant quadrupole excitation of ion oscillations at frequency $(2 - \beta)f$, where β is the characteristic index near the top of the stability region and f is the oscillator frequency. As a result, the performance of QMFs with circular rods such as reproducibility of noble gases isotopic composition, resolution, and

isotopic sensitivity were improved. Compensation for imperfections in QMF electrode fabrication and assembly is achieved by increasing the complexity of the electronics.

In the present work, we emphasize the use of an analytical description of the field created by rounds rods as series of harmonic polynomials. This approach allows not to solve the Laplace equation numerically. We describe the input ion beam by Gaussian random distributions for transverse coordinates and velocities. The limitation of the method used is the requirement for the electrodes to be parallel and cylindrical.

The obtained data may be useful in the development of QMF and MCs based on them.

ACKNOWLEDGEMENTS

The authors gratefully acknowledge the financial support from the Ministry of Science and Higher Education of the Russian Federation in the framework of Agreement No. 075-03-2023-097.

DATA AVAILABILITY STATEMENT

Data sharing not applicable to this article as no datasets were generated or analysed during the current study.

ORCID

Nikolai V. Konenkov https://orcid.org/0000-0002-8873-2497

REFERENCES

1. Dawson PH. *Quadrupole mass spectrometry and its applications*. Vol. 372. AVS Classics in Vacuum Science and Technology; 1995. ISBN: 9781483165042.
2. Dawson PH. Ion optical properties of quadrupole mass filters. In: Marton L, Marton C, eds. *Advances in electronics and electron physics*. Academic Press Inc.; 1980:153-208. doi:10.1016/S0065-2539(08)60260-7
3. Hogan TJ, Taylor S. Performance simulation of a quadrupole mass filter operating in the first and third stability zones. *IEEE Trans Instr Meas*. 2008;57(3):498-508. doi:10.1109/TIM.2007.911632
4. Du Z, Douglas DJ, Konenkov NV. Peak splitting with a quadrupole mass filter operated in the second stability region. *J am Soc Mass Spectrom*. 1999;10(12):1263-1270. doi:10.1016/s1044-0305(99)00100-2
5. Forbes MW, Sharifi M, Croley T, Lausevic Z, March RE. Simulation of ion trajectories in a quadrupole ion trap: a comparison of three simulation programs. *J Mass Spectrom*. 1999;32:1219-1239.
6. Blaum K, Geppert C, Müller P, Nörtershäuser W, Wendt K, Bushaw BA. Peak shape for a quadrupole mass spectrometer: comparison of computer simulation and experiment. *J Mass Spectrom*. 2000;202(1–3):81-89. doi:10.1016/s1387-3806(00)00237-2
7. Gibson JR, Taylor S. Prediction of quadrupole mass filter performance for hyperbolic and circular cross section electrodes. *Rapid Commun Mass Spectrom*. 2000;14(18):1669-1673.
8. Gibson JR, Taylor S. Numerical investigation of the effect of electrode size on the behaviour of quadrupole mass filters. *Rapid Commun Mass Spectrom*. 2001;15(20):1960-1964. doi:10.1002/rcm.469
9. Gibson JR, Taylor S. Asymmetrical features of mass spectral peaks produced by quadrupole mass filters. *Rapid Commun Mass Spectrom*. 2003;17(10):1051-1055. doi:10.1002/rcm.1017
10. Taylor S, Gibson JR. Prediction of the effects of imperfect construction of a QMS filter. *J Mass Spectrom*. 2008;43(5):609-616. doi:10.1002/jms.1356
11. Gibson JR, Evans KG, Taylor S. Modelling mass analyzer performance with fields determined using the boundary element method. *J Mass Spectrom*. 2010;45(4):364-371. doi:10.1002/jms.1720
12. Syed SU, Hogan T, Gibson J, Taylor S. Factors influencing the QMF resolution for operation in stability zones 1 and 3. *J am Soc Mass Spectrom*. 2012;23(5):988-995. doi:10.1007/s13361-012-0348-4
13. Douglas DJ, Konenkov NV. Influence of the 6th and 10th spatial harmonics on the peak shape of a quadrupole mass filter with round rods. *Rapid Commun Mass Spectrom*. 2002;16(15):1425-1431. doi:10.1002/rcm.735
14. Dawson PH, Whetten NR. Non-linear resonances in quadrupole mass spectrometers due to imperfect fields. *Int J Mass Spectr Ion Phys*. 1969;3(1–2):1-12. doi:10.1016/0020-7381(69)80054-9
15. Schulte J, Shevchenko PV, Radchik AV. Nonlinear field effects in quadrupole mass filters. *Rev Sci Instrum*. 1999;70(9):3566-3571. doi:10.1063/1.1149960
16. Takai R, Nakayama K, Saiki W, Ito K, Okamoto H. Nonlinear resonance effects in a linear Paul trap. *J Physical Soc Japan*. 2007;76(1):014802. doi:10.1143/JPSJ.76.014802
17. Antony Joseph MJ, McIntosh DG, Gibson JR, Taylor S. Effects of the source gap on transmission efficiency of a quadrupole mass spectrometer. *Rapid Commun Mass Spectrom*. 2018;32(9):677-685. doi:10.1002/rcm.8094
18. Douglas DJ, Glebova TA, Konenkov NV, Sudakov MY. Spatial harmonics of the field in a quadrupole mass filter with circular electrodes. *Tech Phys*. 1999;44(10):1215-1219. doi:10.1134/1.1259497
19. Konenkov AN, Douglas DJ, Konenkov NV. Spatial harmonics of linear multipoles with round electrodes. *Int J Mass Spectry*. 2010;289(2–3):144-149. doi:10.1016/j.ijms.2009.10.007
20. Konenkov NV. A simulation study of excitation contour of a linear trap with spatial harmonics. *Eur J Mass Spectr*. 2021;27(2–4):94-100. doi:10.1177/14690667211020153
21. Mathematica & Wolfram language fast introduction for math students//Wolfram. Available at: https://www.wolfram.com/language/fast-introduction-for-math-students/en/// (accessed 17.05.2023).
22. Konenkov N, Londry F, Ding C, Douglas DJ. Linear quadrupoles with added hexapole fields. *J am Soc Mass Spectrom*. 2006;17(8):1063-1073. doi:10.1016/j.jasms.2006.03.013
23. Konenkov NV, Kratenko VI. Characteristics of a quadrupole mass filter in the separation mode of a few stability regions. *Int J Mass Spectrom Ion Process*. 1991;108(2–3):115-136. doi:10.1016/0168-1176(91)85029-L
24. Zhao XZ, Xiao Z, Douglas DJ. Overcoming field imperfections of quadrupole mass filters with mass analysis in islands of stability. *Anal Chem*. 2009;81(14):5806-5811. doi:10.1021/ac900711b
25. Gershman DJ, Block BP, Rubin M, Benna M, Mahaffy PR, Zurbuchen TH. Comparing the performance of hyperbolic and circular rod quadrupole mass spectrometers with applied higher order auxiliary excitation. *Int J Mass Spectrom*. 2012;319-320:17-24. doi:10.1016/j.ijms.2012.03.008

How to cite this article: Bugrov PV, Sysoev AA, Konenkov NV. Modelling some rod set imperfections of a quadrupole mass filter. *J Mass Spectrom*. 2023;58(12):e4986. doi:10.1002/jms.4986